J Therm Anal Calorim (2012) 110:127–135
DOI 10.1007/s10973-011-2145-x

# Thermal and kinetic analysis of uranium salts

## Part 2. Uranium (VI) acetate hydrates

**Gülbanu Koyundereli Çılgı · Halil Cetişli · Ramazan Donat**

CEEC-TAC1 Conference Special Issue


**Abstract** In this study the thermal decomposition kinetics of uranyl acetate dehydrate [$UO_2(CH_3COO)_2{\cdot}2H_2O$] were studied by thermogravimetry method in flowing nitrogen, air, and oxygen atmospheres. Decomposition process involved two stages for completion in all atmosphere conditions. The first stage corresponded to the removal of two moles of crystal water. The decomposition reaction mechanism of the second stage in nitrogen atmosphere was different from that in air and oxygen atmospheres. Final decomposition products were determined with X-ray powder diffraction method. According to these data, $UO_2$ is the final product in nitrogen atmosphere, whereas $U_3O_8$ is the final product in air and oxygen atmospheres. The calculations of activation energies of all reactions were realized by means of model-free and modeling methods. Kissinger–Akahira–Sunose (KAS) and Flynn–Wall–Ozawa (FWO) methods were selected for model-free calculations. For investigation of reaction models, 13 kinetic model equations were tested. The model, which gave the highest linear regression, the lowest standard deviation, and an activation energy value which was close to those obtained from KAS and FWO equations, was selected as the appropriate model. The optimized value of activation energy and Arrhenius factor were calculated using the selected model equation. Using these values, thermodynamic functions ($\Delta H^*$, $\Delta S^*$, and $\Delta G^*$) were calculated.

**Keywords** Uranyl acetate · Activation energy · Model-free methods · Kinetic model

G. K. Çılgı (✉) · H. Cetişli · R. Donat
Department of Chemistry, Faculty of Science and Arts, Pamukkale University, 20070 Denizli, Turkey
e-mail: gkcilgi@gmail.com

## Introduction

There is a growing interest in uranium compounds due to the possibility of their applications in nuclear and medicine industry. In addition, they have very important environmental aspects. Therefore, many investigators have studied uranium compounds, especially uranyl carboxylates.

Duval and his co-workers were the first researchers who studied thermal behavior of uranyl acetate dihydrate. According to them, uranyl acetate dihydrate shows thermal stability up to 100 °C and loses two crystal water molecules between 100 and 159 °C. Anhydrous salt remains stable up to 247 °C and then starts to decompose slowly at this temperature, rapidly at 380 °C, and explosively at 412 °C [1].

Clough et al. [2] published a detailed and systematized study of thermal decomposition of uranyl acetate in nitrogen and air atmospheres. The changes in the specific surface area and density during decomposition were investigated. Some residues of decomposition were identified, and the mechanism of decomposition was suggested. Those authors studied decomposition kinetics using isothermal methods.

In 1973, Yanachkova and Staevsky repeated the same study in air atmosphere. According to these authors, dehydration occurs between 95 and 140 °C. Anhydrous salt was stable up to 245 °C and then starts to decompose slowly. Mass loss value reaches significant values within the temperature range between 325 and 400 °C. In this stage, chemical bonds are broken, and acetate groups are removed. A slightly endothermic peak was observed for this stage. However, this peak was overlapped large exothermic peak at 400 °C. This stage belongs to oxidation. Authors reexamined oxidation region with lower heating rates and observed an intermediate product which has an orange color. The authors used IR spectroscopy technique

and explained that this intermediate product is $UO_3$. At the completion of the thermal analysis, the authors collected the final decomposition residue and identified it as $U_3O_8$ using X-ray technique [3].

Donava et al. were the most important contributors to thermal analysis of double salts of uranyl acetate with non-metallic cations. They conducted the thermal analysis in air atmosphere and found that the compound decomposed to $UO_2$ first and then oxidized to $UO_3$ and $U_3O_8$, respectively [4–6].

Sampath et al. [7] investigated the thermal decomposition of double salts of uranyl acetate with metallic cations and determined the intermediate and final products.

As noted above, there has been limited research effort devoted to this field. These studies were confined to thermal behavior of uranyl acetate salts, but kinetic studies were not reported. Therefore, there is a gap in the academic literature about kinetic analysis of each decomposition stage of uranyl acetate salts. However, the kinetic and thermodynamic findings play an important role in solid-state chemistry. This situation has indicated a need for further studies on the thermal decomposition kinetics of uranyl acetate.

In this study, thermal decomposition of uranyl acetate dihydrate ($UO_2(CH_3COO)_2{\cdot}2H_2O$) compound has been examined in detail; and reaction kinetic and thermodynamic parameters were determined. The reaction enthalpy value of dehydration stages were calculated from differential scanning calorimeter (DSC) and differential thermal analysis (DTA) peak areas. The activation energy value for each stage was calculated via Kissinger–Akahira–Sunose (KAS) and Flynn–Wall–Ozawa (FWO) integral model-free equations. The alterations of activation energies with respect to the decomposition fraction, atmospheric conditions, and the method were investigated. Once the activation energy has been determined, it was possible to find the kinetic model which best describes thermogravimetry (TG) curve of the measurement. Thirteen model equations were used to fit kinetic curves. The model, which gave the highest linear regression, the lowest standard deviation, and which resulted in an activation energy value which was close to those obtained from KAS and FWO equations, was selected as the appropriate model. The optimized value of activation energy and Arrhenius factor were calculated with this selected equation. Using these optimized values, other thermodynamic functions ($\Delta H^*$, $\Delta S^*$, and $\Delta G^*$) were calculated.

## Theory

There are different methods in the academic literature for the calculations of activation energy values of decomposition reactions. These methods are classified as integral methods [8–12] and differential methods [13–16].

In this study, we selected KAS and FWO methods which are well known as integral methods in the academic literature. The final equations of these methods for model-free calculations are as follows:

KAS equation:

$$\ln\frac{\beta}{T^2} = \left[\ln\frac{AR}{g(\alpha)E}\right] - \frac{E}{R}\times\frac{1}{T}, \tag{1}$$

and FWO equation:

$$\ln\beta = \left[\frac{A\cdot E}{R\cdot g(\alpha)}\right] - 5.3305 - 1.05178\frac{E}{R}\times\frac{1}{T}, \tag{2}$$

where $\alpha$ corresponds to the degree of conversion, $A$ stands for the pre-exponential factor, $E$ denotes the activation energy, $g(\alpha)$ represents the differential conversion function, and $R$ is the gas constant.

For determining the constant $\alpha$, the plots of $\ln\beta/T^2$ versus $1/T$ (for KAS equation) and $\ln\beta$ versus $1/T$ (for FWO equation) are obtained from TG graphs. The $\ln\beta/T^2$ versus $1/T$ plots and $\ln\beta$ versus $1/T$ plots, which are recorded at different heating rates, both should form a straight line with a slope that allows for an evaluation of the activation energy.

For the determination of reaction kinetic model, KAS and FWO equations were reorganized as "Composite Method I" and "Composite Method II," which are already known in the academic literature, as shown below [17, 18]:

Modeling KAS equation (Composite Method I—CM I):

$$\ln\frac{g(\alpha)}{T^2} = \left[\ln\frac{AR}{\beta E}\right] - \frac{E}{R}\times\frac{1}{T}. \tag{3}$$

Modeling FWO equation (Composite Method II—CM II):

$$\ln g(\alpha) = \left[\frac{A\cdot E}{\beta\cdot R}\right] - 5.3305 - 1.05178\frac{E}{R}\times\frac{1}{T}. \tag{4}$$

Thus, the dependence of $\ln[g(\alpha)/T^2]$ (while modeling with KAS method) or $\ln[g(\alpha)]$ (while modeling with FWO method) on $1/T$ for different $\alpha$ values at a constant $\beta$ value must produce a single master straight line for the correct form of $g(\alpha)$. The activation energy and the pre-exponential factor values can be determined for each model functions, $g(\alpha)$, which are already well known in the academic literature [19, 20]. The kinetic model function, which gave the highest regression analysis, the lowest standard deviation, and which produced an activation energy value that showed good agreement to those obtained from model-free KAS and FWO equations, was selected as the appropriate model.

The entropy of activation, $\Delta S^*$, can be obtained by the following equation:

$$A = (kT_{avg}/h) \times e^{\Delta S^*/R}, \quad (5)$$

where $k$ stands for the Boltzmann constant, $h$ denotes the Planck's constant, and $T_{avg}$ corresponds to average reaction temperature.

Hence,

$$\Delta H^* = E_a - RT_{avg}, \quad (6)$$

where $E_a$ gives the activation energy that is obtained from the slope of the graphs of composite methods for the selected model. The changes in the enthalpy $\Delta H^*$ and Gibbs free energy $\Delta G^*$ for the activated complex formation from the reagent can be determined by the well-known thermodynamic equation, as follows:

$$\Delta G^* = \Delta H^* - T_{avg}\Delta S^*. \quad (7)$$

## Experimental

$UO_2(CH_3COO)_2{\cdot}2H_2O$ was obtained from Merck. All of the TG, differential thermogravimetry (DTG), and DTA curves were obtained simultaneously using a Shimadzu DTG-60H Thermal Analyzer. DSC measurements were performed using a Shimadzu DSC-60H device. The measurements were carried out in flowing nitrogen, air, and oxygen atmospheres (100 mL/min), and temperature ranged from 25 to 500 °C in an alumina crucible. Highly sintered $Al_2O_3$ was used as the reference material. The lower heating rates ($\beta$) were chosen (6, 4, and 2 °C/min) to distinguish each reaction and to determine the reaction's initial and final temperatures exactly. Moreover, lower heating rates allow for the completion of the reaction and complete removal of the volatile products from the solid material. The sample mass ($w_o$) ranged from 11 to 12 mg. Before carrying out the experiments, it is essential to calibrate the balance for buoyancy effects for the quantitative estimation of mass changes. The material chosen for the investigation of such effects was silver. The temperature was calibrated measuring the melting points of indium and tin provided by Shimadzu. All experiments were performed three times to obtain statistical significance, and the results showed good consistency with the smaller variations (maximum ±3 kJ/mol) in the kinetic parameters.

The X-ray powder diffraction patterns were obtained using Rigaku Miniflex X-ray diffractometer, equipped with Cu Kα radiation source.

## Results and discussions

### Thermal analysis of $UO_2(CH_3COO)_2{\cdot}2H_2O$

The TG and DTA curves that were obtained in all the heating rates and in all atmospheres for the experiments are presented in Fig. 1. The thermal analysis results obtained from the evaluation of these curves are summarized in Table 1. It is found that the decomposition of uranyl acetate hydrate consists of two stages. The first stage corresponds to dehydration reaction and shows endothermic character in all atmospheres. The second stage was attributed to decomposition of acetate groups and formation of uranium oxide. This reaction shows endothermic character in nitrogen atmosphere, but exothermic character in air and oxygen atmospheres.

Reaction temperature ranges were determined by evaluating not only the TG graphs, but also the minimum points of variation of activation energy versus decomposition fraction as shown in the "Kinetic analysis of $UO_2(CH_3COO)_2{\cdot}2H_2O$" section. The peak temperatures and the temperature ranges of all reactions increased with the increase of heating rate-$\beta$, which was programmed during the thermal analysis. The reason for this shift is the time needed for achieving a certain temperature decreases. This effect was observed in the other thermal analysis studies in the academic literature [21–24].

The experimental mass loss percentage (avg 8.492% in all heating rates and all atmospheres) due to dehydration of two molecules of water is perfectly compatible with theoretical value (8.493%). The dehydration reaction starts at 371 K and finishes at 397 K averagely in all atmospheres and heating rates. The calculated enthalpy of dehydration reaction does not vary significantly with respect to the heating rate, $\beta$, and the reaction atmosphere, and results in an average value of 166.830 or 83.42 kJ/mol of water. This value is higher than the evaporation enthalpy of the water (40.60 kJ/mol), the molecules of which are chemically bonded to the compound.

Decomposition stages of anhydrite uranyl acetate occur with a different mechanism in nitrogen atmosphere compared to air and oxygen atmospheres. In nitrogen atmosphere, the reaction shows endothermic characteristic and occurs in the 395–641 K temperature range in average. $UO_2$ is the final product of this reaction. Results of X-ray powder diffraction patterns of the final product (Fig. 2) and the harmony of experimental mass loss percentage value (27.289%) with that of the theoretical (27.837%) proved that final decomposition product is $UO_2$ ([25], $UO_2$ File No. 75-0420).

Contrary to the decomposition reaction in nitrogen atmosphere, the decomposition reaction shows exothermic characteristic in air and oxygen atmospheres. $UO_3$ occurs as a first decomposition product, but close to the finishing temperature (in air atmosphere: 590–622 K, in oxygen atmosphere: 610–645 K), a sudden collapse happens and $UO_3$ turns to $U_3O_8$. Theoretic mass loss percentage value (25.322%) is compatible with those of experimental values (in air atmosphere: 25.404%; and in oxygen atmosphere:

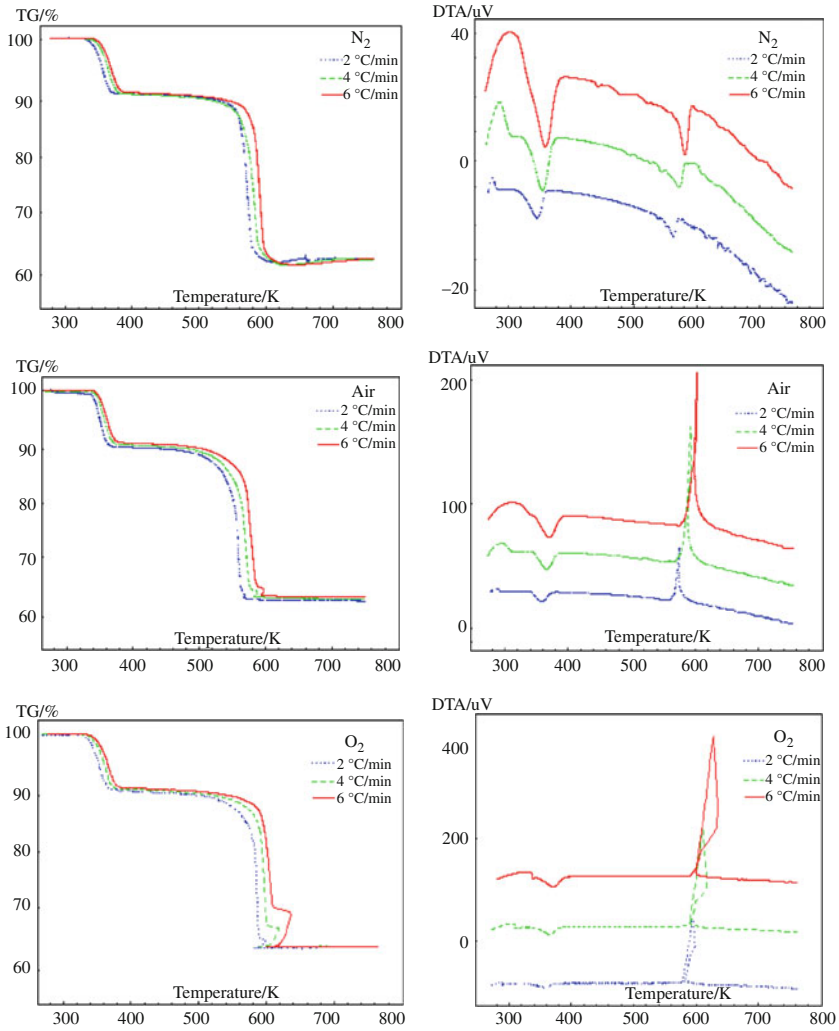


**Fig. 1** TG and DTA curves of $UO_2(CH_3COO)_2{\cdot}2H_2O$ in all atmospheres and heating rates

**Table 1** The mass loss data for the decomposition of $UO_2(CH_3COO)_2{\cdot}2H_2O$ in all atmospheres at different heating rates

| Atm. | Reaction | Dehydration | | | | Decomposition | | | |
|---|---|---|---|---|---|---|---|---|---|
| | $\beta$/°C/min | 2 | 4 | 6 | Avg | 2 | 4 | 6 | Avg |
| $N_2$ | $T_i$K | 344 | 351 | 358 | 351 | 385 | 396 | 404 | 395 |
| | $T_f$K | 385 | 396 | 404 | 395 | 628 | 641 | 654 | 641 |
| | $T_{peak}$K | 373.98 | 382.12 | 386.84 | 380.98 | 587.45 | 596.98 | 606.13 | 596.85 |
| | $\%\Delta w$ | 8.499 | 8.526 | 8.469 | 8.498 | 27.047 | 27.408 | 27.412 | 27.289 |
| Air | $T_i$K | 362 | 367 | 368 | 366 | 400 | 410 | 420 | 410 |
| | $T_f$K | 391 | 400 | 410 | 400 | 773 | 773 | 773 | 773 |
| | $T_{peak}$K | 377.63 | 385.14 | 389.17 | 383.98 | 594.86 | 612.39 | 622.56 | 609.94 |
| | $\%\Delta w$ | 8.465 | 8.499 | 8.509 | 8.491 | 25.404 | 25.371 | 25.438 | 25.404 |
| $O_2$ | $T_i$K | 348 | 352 | 357 | 352 | 396 | 400 | 410 | 402 |
| | $T_f$K | 386 | 394 | 405 | 395 | 773 | 773 | 773 | 773 |
| | $T_{peak}$K | 374.16 | 382.21 | 388.57 | 381.65 | 608.42 | 623.96 | 640.89 | 624.42 |
| | $\%\Delta w$ | 8.493 | 8.504 | 8.463 | 8.487 | 25.322 | 25.417 | 25.652 | 25.464 |

25.464%) for decomposition of acetate groups and formation of the $U_3O_8$ product. Also this conclusion is supported both by the X-ray powder diffraction pattern of the residue of thermal decomposition (Fig. 2) and by the color of the residue which is dark green [25, $U_3O_8$ File No. 31-1424].

## Kinetic analysis of $UO_2(CH_3COO)_2{\cdot}2H_2O$

First, we have studied a combination of dehydration and decomposition reactions to determine the temperature range accurately. Figure 3 presents the variation of activation energy with respect to the decomposition ratio-$\alpha$ in all atmospheres.

As seen from the Fig. 3, two reactions can be clearly separated. The temperature and time ranges for dehydration and decomposition reactions were determined using the minimum points in $E_a$–$\alpha$ graphs. The activation energy values changed suddenly at the termination of decomposition reaction in air and oxygen atmospheres. This situation is due to a conversion of $UO_3$ to $U_3O_8$ at the mentioned temperature region.

After that separation, the activation energy value of each stages were calculated using the two model-free methods, and their variation behaviors with respect to the decomposition ratio are presented in Fig. 4.

The activation energy values which were calculated by means of the two methods are perfectly compatible with

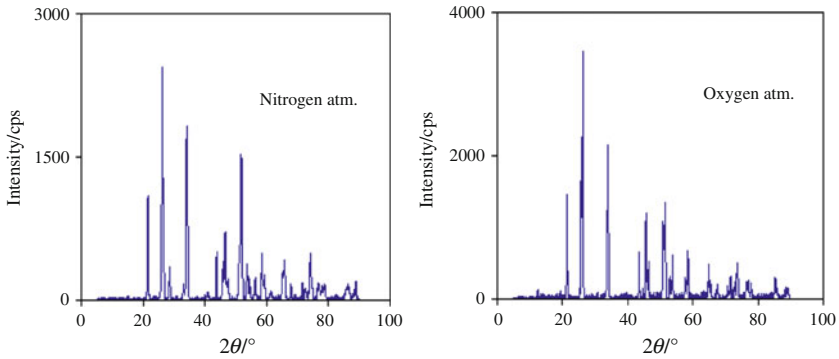


**Fig. 2** X-ray powder diffraction patterns of the final residue of thermal decomposition in nitrogen and oxygen atmospheres

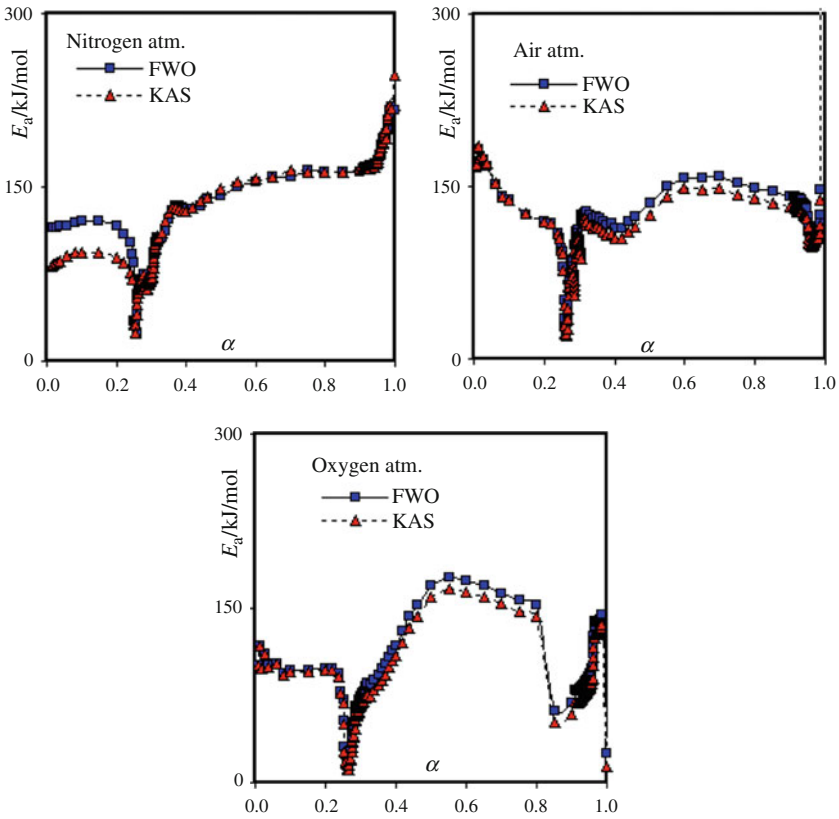


**Fig. 3** Variation of activation energy with respect to the decomposition ratio-$\alpha$, for combination of dehydration and decomposition reactions

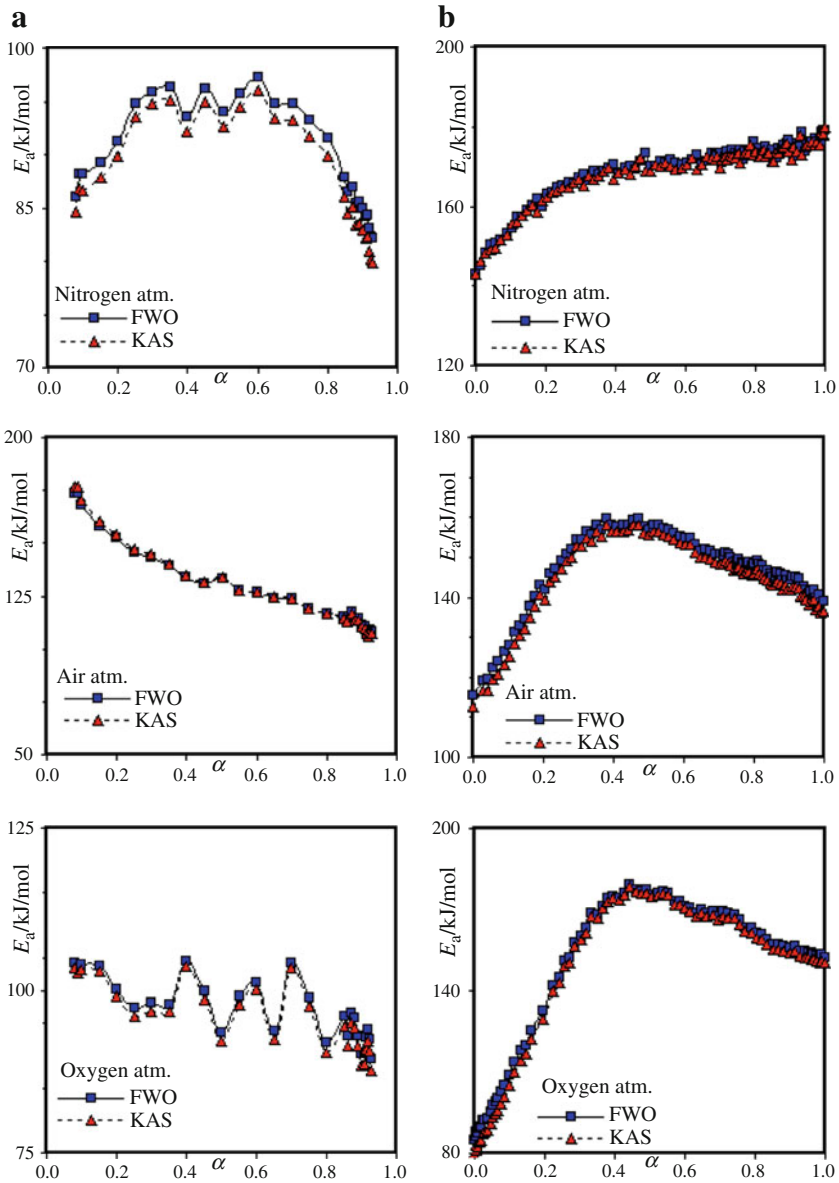


**Fig. 4** Variations of activation energy values of dehydration (**a**) and decomposition (**b**) reactions with α in all atmospheres

**Table 2** The average activation energy values calculated using composite methods and model-free methods (KAS–FWO) for dehydration and decomposition reactions

| React. | Atmospheric condition | Model | Composite Method I | | | | Composite Method II | | | |
|---|---|---|---|---|---|---|---|---|---|---|
| | | | $R^2$ | $S$ | $E_a$/kJ/mol | KAS $E_a$/kJ/mol | $R^2$ | $S$ | $E_a$/kJ/mol | FWO $E_a$/kJ/mol |
| Dehydration | $N_2$ | $A_{1.5}$ | 0.996 | 1.98 | 80.673 | 88.139 | 0.996 | 1.784 | 82.643 | 89.774 |
| | Air | $A_{1.5}$ | 0.982 | 9.681 | 103.058 | 129.702 | 0.984 | 9.128 | 104.025 | 129.375 |
| | $O_2$ | $A_{1.5}$ | 0.997 | 2.472 | 86.030 | 97.103 | 0.998 | 2.249 | 87.746 | 97.103 |
| Decomposition | $N_2$ | $A_3$ | 0.994 | 25.192 | 133.109 | 168.986 | 0.995 | 23.997 | 135.969 | 169.629 |
| | Air | $A_4$ | 0.988 | 5.491 | 152.081 | 143.510 | 0.990 | 5.167 | 153.972 | 145.785 |
| | $O_2$ | $A_3$ | 0.976 | 52.434 | 145.586 | 142.717 | 0.980 | 50.073 | 147.837 | 145.046 |

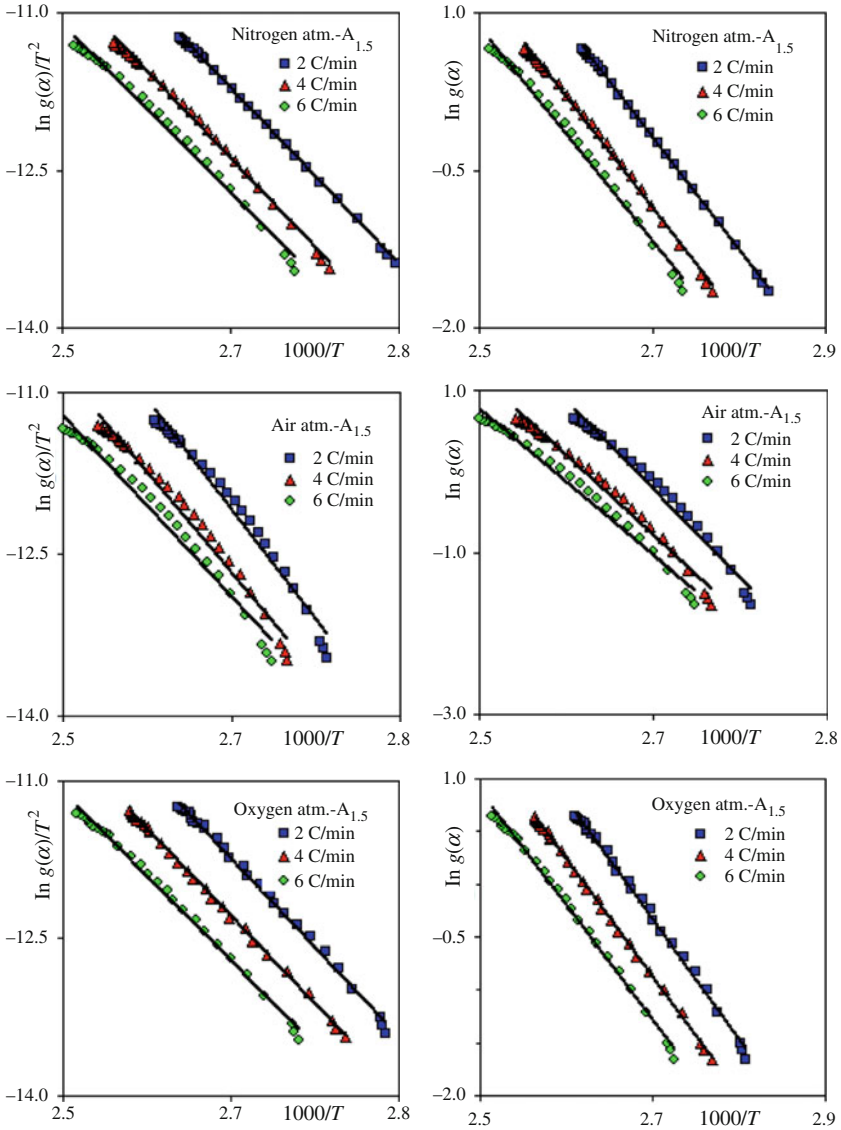


**Fig. 5** The most appropriate model graphs of dehydration reaction in all atmospheres (*left side* for CM I and *right side* for CM II)

**Table 3** Thermodynamic parameters of dehydration and decomposition reactions

| React. | Atmospheric condition | Method | Model | $E_a$/kJ/mol | ln $A$ | $\Delta H^*$/kJ/mol | $\Delta S^*$/J/mol K | $\Delta G^*$/kJ/mol |
|---|---|---|---|---|---|---|---|---|
| Dehydration | $N_2$ | CM I | $A_{1.5}$ | 80.673 | 24.183 | 77.522 | −45.845 | 94.918 |
| | | CM II | $A_{1.5}$ | 82.643 | 24.907 | 79.492 | −39.828 | 94.605 |
| | Air | CM I | $A_{1.5}$ | 103.058 | 31.078 | 99.886 | 11.428 | 95.608 |
| | | CM II | $A_{1.5}$ | 104.025 | 31.383 | 100.833 | 13.904 | 95.574 |
| | $O_2$ | CM I | $A_{1.5}$ | 86.030 | 25.890 | 82.873 | −31.671 | 94.927 |
| | | CM II | $A_{1.5}$ | 87.746 | 26.498 | 84.590 | −26.617 | 94.721 |
| Decomposition | $N_2$ | CM I | $A_3$ | 133.109 | 25.064 | 128.148 | −42.297 | 153.313 |
| | | CM II | $A_3$ | 135.969 | 25.734 | 131.008 | −36.727 | 152.852 |
| | Air | CM I | $A_4$ | 152.081 | 29.132 | 147.124 | −8.467 | 152.200 |
| | | CM II | $A_4$ | 153.972 | 29.526 | 149.017 | −5.190 | 152.134 |
| | $O_2$ | CM I | $A_3$ | 145.586 | 26.981 | 140.591 | −26.411 | 155.800 |
| | | CM II | $A_3$ | 147.837 | 27.538 | 142.842 | −21.786 | 155.311 |

each other and present similar variations especially in air atmosphere for the dehydration reaction. In nitrogen atmosphere, the activation energy values increase with dehydration ratio up to $\alpha = 0.35$ ,then show fluctuations up to $\alpha = 0.60$, and then decrease with increasing dehydration ratio. In air atmosphere, activation energy values decrease persistently with increasing dehydration ratio. In oxygen atmosphere, activation energy values show fluctuations with increasing dehydration ratio. The average activation energy values are 89.774, 97.103, and 129.375 kJ/mol in nitrogen, oxygen and air atmospheres, respectively.

Figure 4b shows the variation graphs for the activation energy values versus the decomposition ratio. It was observed that the variations of activation energy versus the decomposition ratio were similar in both air and oxygen atmospheres. Activation energy values increased with an increase in the decomposition ratio, and reached up to a maximum for decomposition ratio values ranging between 0.50 and 0.55. After reaching that maximum, the values of activation energy decreased gradually. $E_a$–$\alpha$ variation graph partially differentiated in the nitrogen atmosphere. The activation energy values tended to increase with increasing $\alpha$ and reached a maximum value (179.968 kJ/mol) at the end of decomposition. Also, in nitrogen atmosphere, the average activation energy value is (169.308 kJ/mol) higher than that in air and oxygen atmospheres (144.782 kJ/mol). These results support the hypothesis that the decomposition mechanisms and decomposition products are different in nitrogen atmosphere compared with air and oxygen atmospheres.

After the completion of these model-free calculations, we investigated the reaction models with modeling (composite) methods. We identified the model which gave the highest regression analysis, the lowest standard deviation, and with an activation energy value that shows good agreement with those obtained from model-free KAS and FWO equations and selected it as the appropriate model. Calculated activation energy, standard deviation, and regression analysis values from the selected model that fit best to the dehydration and decomposition reactions are presented in Table 2. For comparison, the activation energy values, which were calculated using model-free KAS and FWO equations, are also presented in the same table.

The most appropriate model equation is $A_{1.5}$ for dehydration reaction in all atmospheres. This model corresponds to nucleation and recrystallization. This can be seen from the graphs of the selected model for the dehydration reaction in all the atmospheres of the experiments are presented in Fig. 5. Similarly, most of the dehydration reactions were explained with nucleation mechanism in the literature [26–28].

Decomposition reaction is compatible with $A_3$ model in nitrogen and oxygen atmospheres. $A_4$ model is more appropriate than $A_3$ model for air atmosphere. Although both models represent the nucleation event, only the formation of the core is different. Clough et al. [2] investigated the thermal decomposition of uranyl acetate under isothermal conditions. They observed the compound during decomposition with electron microscopy and observed nucleation. Nucleation event is frequently used to explain the decomposition mechanism. Gabal [17] found that $A_2$ and $A_3$ models were the most appropriate models for defining cadmium and zinc oxalate decomposition reactions. Likewise, decomposition of anhydrous uranyl oxalate, which occured in two steps, was explained using nucleation models ($A_3$) [29].

After the determination of reaction model, we calculated other thermodynamic parameters using the selected model equations. Table 3 presents these values.

The average calculated values of $\Delta H^*$, $\Delta S^*$, and $\Delta G^*$ for decomposition reaction are, respectively, 129.578 kJ/mol, −39.512 J/mol K, and 153.083 kJ/mol in nitrogen atmosphere; 148.071 kJ/mol, −6.828 J/mol K, and 152.167 kJ/mol in air atmosphere; 141.716 kJ/mol, −24.098 J/mol K, 155.555 kJ/mol in oxygen atmosphere. The entropy of activation ($\Delta S^*$) value for decomposition reaction is negative in all atmospheres. It means that the corresponding activated complexes had higher degrees of arrangement compared to their initial states. Hence, the removal of acetate groups may be interpreted as a slow-stage reaction. Furthermore, the positive value of $\Delta G^*$ shows that decomposition depends on introduction of heat, and it is a non-spontaneous process [30, 31].

## Conclusions

Thermal decomposition of the $UO_2(CH_3COO)_2{\cdot}2H_2O$ was studied using TG method in nitrogen, air, and oxygen atmospheres. It was found that the compound decomposes to oxide residues in two stages which correspond to dehydration and decomposition reactions. For the determination of reaction temperature ranges, not only TG graphs, but also the minimum points of variation of activation energy versus decomposition fraction were used.

While dehydration reactions took place with the same mechanism in all atmospheres, atmospheric conditions were found to be very important for the decomposition reactions. In nitrogen atmosphere, the decomposition showed an endothermic character, and the reaction attained completion with the formation of $UO_2$ oxide product. In air and oxygen atmospheres, the decomposition showed an exothermic character and anhydrous uranyl acetate decomposed initially to $UO_3$ than finally to $U_3O_8$ oxide products. Final decomposition products were verified by X-ray diffraction patterns.

All the involved reaction stages were investigated in detail. The activation energies of the dehydration and decomposition reactions were calculated using the model-free equations; the KAS and FWO methods and graphs

which showed the variation behavior with respect to the decomposition ratio were prepared. Activation energy values calculated by these two methods were compatible with each other. In air and oxygen atmospheres, the activation energy values of decomposition reaction increased with an increase in decomposition ratio $\alpha$ up to 0.50–0.55, and then decreased with decreasing $\alpha$ continuously, which corresponded to a nucleation and growth kinetic mechanism. Modeling studies have confirmed this finding. Kinetic model equations were determined for other reactions (the decomposition reaction in nitrogen atmosphere and the dehydration reaction in all atmospheres). The other thermodynamic parameters were calculated from the selected model equations. These thermodynamic functions were consistent with kinetic parameters.

Certain conclusions can be derived concerning the mechanisms and characteristics of decomposition processes using the apparent activation energy, pre-exponential factor, and the changes of entropy, enthalpy, and Gibbs free energy data. The kinetic and thermodynamic data play an important role in theoretical studies as well as industrial applications. Thus, the findings of this study will guide further studies on uranyl acetate dihydrate and will contribute to the solution of various scientific and practical problems involving the participation of solid phases.

**Acknowledgements** This study was financially supported by the Turkish Scientific and Technological Research Council through Grant # 107T293(TBAG-HD/282) and by Pamukkale University through Grant # 2009FBE001.

## References

1. Duval C, Wadier C, Servigne Y. Sur la stabilité thermique des étalons analytiques vii. Anal Chim Acta. 1959;20:263–7.
2. Clough PS, Dollimore D, Grundy P. The thermal decomposition of uranyl acetate. J Inorg Nucl Chem. 1969;31:361–70.
3. Yanachkova IM, Staevsky M. Thermal decomposition of uranyl acetate. J Mater Sci. 1973;8:606–10.
4. Donova I, Aleksovska S, Stefov V. Synthesis, characterization and thermal decomposition of pyridinium uranyl acetate. Thermochim Acta. 2000;348:169–74.
5. Donova I, Stefov V, Aleksovska S. Synthesis, characterization and thermal decomposition of hydroxylammonium uranyl acetate. J Therm Anal Calorim. 2001;63:125–32.
6. Aleksovska S, Donova I, Stefov V. Synthesis, identification, structural and thermal stability investigations on bipyridinium uranyl acetate. Thermochim Acta. 2002;389:71–7.
7. Sampath S, Kulkarni NK, Jayadevan NC. X-ray and thermal studies on uranyl acetates of zinc, magnesium and nickel. J Thermal Anal. 1989;35:1089–95.
8. Ozawa T. Kinetic analysis of derivative curves in thermal analysis. J Thermal Anal. 1970;2:301.
9. Çılgı GK, Cetişli H. Thermal decomposition kinetics of aluminum sulfate hydrate. J Therm Anal Calorim. 2009;98:855–61.
10. Boonchom B. Kinetic and thermodynamic studies of $MgHPO_4 \cdot 3H_2O$ by non-isothermal decomposition data. J Therm Anal Calorim. 2009;98:863–71.
11. Rejitha KS, Mathew S. Thermoanalytical investigations of tris(ethylenediamine)nickel(II) oxalate and sulphate complexes: TG–MS and TR–XRD studies. J Therm Anal Calorim. 2010;102:931–9.
12. Ocakoğlu K, Emen FM. Thermal analysis of cis-(dithiocyanato)(1,10-phenanthroline-5,6-dione)(4,4′-dicarboxy-2,2′-bipyridyl)ruthenium(II) photosensitizer. J Therm Anal Calorim. 2011;104:1017–22.
13. Vlase T, Vlase G, Birta N, Doca N. Comparative results of kinetic data obtained with different methods for complex decomposition steps. J Therm Anal Calorim. 2007;88:631–5.
14. Kök MV, Gundogar AS. Effect of different clay concentrations on crude oil combustion kinetics by thermogravimetry. J Therm Anal Calorim. 2010;99:779–83.
15. Kök MV, Guner G, Bagcı S. Combustion kinetics of oil shales by reaction cell experiments. Oil Shale. 2008;25:5–18.
16. Kök MV, Smykatz-Kloss W. Characterization, correlation and kinetics of dolomite samples as outlined by thermal methods. J Therm Anal Calorim. 2008;91:565–8.
17. Gabal MA. Non-Isothermal studies for the decomposition course of $CdC_2O_4$–$ZnC_2O_4$ mixture in air. Thermochim Acta. 2004;412:55–62.
18. Budrugeac P, Segal E. On the use of Diefallah's composite integral method for the non-isothermal kinetic analysis of heterogeneous solid–gas reactions. J Therm Anal Calorim. 2005;82:677–80.
19. Wendlant Wesley WM. Thermal Analysis. 3rd ed. New York: John Wiley; 1986.
20. Vyazovkina S, Burnhamb AK, Criadoc JM, Pérez-Maquedac LA, Popescud C, Sbirrazzuolie N. ICTAC Kinetics Committee recommendations for performing kinetic computations on thermal analysis data. Thermochim Acta. 2011;520:1–19.
21. Kök MV. Heating rate effect on the DSC kinetics of oil shales. J Therm Anal Calorim. 2007;90:817–21.
22. Kaljuvee T, Rudjak I, Edro E, Trikkel A. Heating rate effect on the thermal behavior of ammonium nitrate and its blends with limestone and dolomite. J Therm Anal Calorim. 2009;97:215–21.
23. Sanders JP, Gallagher PK. Kinetic analysis using simultaneous TG/DSC measurements. Part I: decomposition of calcium carbonate in argon. Thermochim Acta. 2002;388:115–28.
24. Andricic B, Kovacic T, Klaric I. Kinetic analysis of the thermooxidative degradation of poly(vinyl-chloride) in poly(vinyl chloride)/methyl methacrylate–butadiene–styrene blends 2. Nonisothermal degradation. Polym Degrad Stab. 2003;79:265–70.
25. The International Centre for Diffraction Data File No. 75-0420 and 31-1424.
26. Favergeon L, Pijolat M, Helbert C. A mechanism of nucleation during thermal decomposition of solids. J Mater Sci. 2008;43:4675–83.
27. Galwey AK, Spinicci R, Guarini GT. Nucleation and growth process occurring during the dehydration of certain alums: the generation, the development and the function of the reaction interface. Proc R Soc Lond A 1981;378:477–505.
28. Koga N, Tanaka H. A physico-geometric approach to the kinetics of solid-state reactions as exemplified by thermal dehydration and decomposition of inorganic solids. Thermochim Acta. 2002;388:41–61.
29. Cetisli H, Koyundereli Çılgı G, Donat R. Thermal and kinetic analysis of uranium salts. Part 1 uranium (VI) oxalate hydrates. J Therm Anal Calorim. 2011. doi: 10.1007/s10973-011-1826-9.
30. Boonchom B, Danvirutai C. Kinetics and thermodynamics of thermal decomposition of synthetic $AlPO_4 \cdot 2H_2O$. J Therm Anal Calorim. 2009;98:771–7.
31. Boonchom B. Kinetics and thermodynamic properties of the thermal decomposition of manganese dihydrogenphosphate dihydrate. J Chem Eng Data. 2008;53:1553–8.